

EFFECTS OF WINDS AND WAVES ON THE EQUATORIAL ELECTROJET

C.A. Reddy

Planetary Atmospheres Branch/Code 914
NASA/Goddard Space Flight Center
Greenbelt, MD 20771, U.S.A.

Height-varying winds associated with the tides and acoustic-gravity waves within the altitude-latitude region of the equatorial electrojet (EEJ) generate electric fields, currents and ion convergences through their local interactions with the ionospheric plasma. Considerable deviations of the height and latitude structures of the EEJ from its "normal" structures take place rather frequently from the above effects. The current status of knowledge on this important aspect of the equatorial electrojet is reviewed. The feasibility and the usefulness of deducing the height-varying winds in the EEJ from the measured electric field structures caused by them are emphasized.

EFEITOS DE VENTOS E ONDAS SOBRE O ELETROJATO EQUATORIAL *Ventos que variam com altura, marés atmosféricas e ondas de gravidade na faixa de altitude e latitude do Eletrojato Equatorial geram campos elétricos e correntes elétricas através de uma interação local com o plasma ionosférico. Desvios consideráveis podem ocorrer nos valores normais médios dentro do Eletrojato por causa dos elementos acima. Faz-se uma revisão do estudo do conhecimento destes efeitos no Eletrojato. Dá-se ênfase ao processo de deduzir os ventos, variáveis com altura, a partir dos campos elétricos observados no Eletrojato, avaliando se o processo é factível e útil.*

INTRODUCTION

The Equatorial Electrojet (EEJ) is a relatively intense electric current flowing in the magnetic east-west direction within a band of a few degrees on either side of the magnetic dip equator where its intensity maximizes around 1100 LT (Fig. 1(a)). In altitude, 90% or more of the current flows in the 90-130 km altitude range, with an approximate parabolic shape for the height structure of the current density and with its maximum in the 102-108 km range (Fig. 1(b)). The electrojet current is driven by a nearly

vertical polarization electric field E_p which is orthogonal to the geomagnetic field lines in the magnetic meridional plane (Fig. 1(c)). But E_p is generated by a large scale, height-invariant, curl-free east-west electric field E_y originating in the dynamo action of the global scale wind system(s) in the thermosphere. During magnetically disturbed periods, an additional contribution to E_y comes from the disturbance electric fields at high latitudes penetrating to the equatorial latitudes through the dynamo region. $E_p(z)$ at any altitude is related to E_y as:

$$E_p(z) = \frac{\int \sigma_2(z) ds}{\int \sigma_1(z) ds} E_y \approx \frac{\sigma_2(z)}{\sigma_1(z)} E_y. \quad (1)$$

where σ_1, σ_2 are Pedersen and Hall conductivities and the integration is done along the length of a magnetic field line s . Since the EEJ current comprises predominantly of the $\bar{E}_p \times \bar{B}$ Hall drift of electrons, where \bar{B} is the geomagnetic field induction, the current density has a height structure at the dip equator which is similar to that of E_p (see Fig. 1(d)). The details of the various aspects of the equatorial electrojet can be found in the papers by Kane (1976), Mayaud (1977), Forbes (1981), Rastogi (1989), Reddy (1977, 1981, 1989), Richmond (1973), Anandarao and Raghavarao (1987), Fejer and Kelley (1980) and Farley (1985) and the references therein.

The effect of the local interaction of neutral winds within the EEJ was considered negligible for a long time. But the significance of this effect has been recognized increasingly in the last two decades starting from the quantitative treatment of this effect by Kato (1973) and Richmond (1973). It is now accepted that very substantial changes in the height and latitude structures of the EEJ take place due to the local interaction of height-varying winds in the EEJ (e.g., see Fambitakoye et al., 1976; Reddy and Devasia, 1981). In this paper, we present an overview of the effects of winds and waves in the equatorial electrojet.

EFFECT OF HEIGHT-INVARIANT ZONAL WIND

Fig. 2(a) shows the Pedersen drift of ions (μ_1) relative to electrons and the Hall drift of electrons (μ_2) relative to ions in the 85-165 km height range due to a constant 1.0 mV/m electric field. The rapid decrease of μ_2 above 115 km and the large decrease of μ_1 on either side of its maximum near 130 km are conducive to the build-up of polarization electric fields in this height range, because electric fields generate

substantial Hall drifts of electrons and winds generate substantial ion drifts in this height region. Fig. 2(b) shows schematically how a large scale eastward electric field E_y (+ve eastward) gives rise to an upward polarization electric field E_p in the magnetic meridional plane in a direction perpendicular to \bar{B} through the differential upward Hall drift of electrons, which slow down rapidly above 115 km. The $\bar{E}_p \times \bar{B}$ drift of electrons in the westward direction contributes predominantly to the daytime current in the EEJ, with a small contribution coming from the Pedersen drift of ions due to E_y . Due to their high collision rate with the neutrals, ions move essentially with the neutral wind velocity U_y in the east-west direction, with the ion velocity V_{iy} becoming progressively smaller than the neutral wind velocity above about 115 km altitude. This neutral wind-generated ion motion gives rise to a polarization electric field E_w , which is also orthogonal to \bar{B} in the magnetic meridional plane, as shown schematically in Fig. 2(c).

The electron Hall drift is altered from $(\bar{E}_p \times \bar{B})/B^2$ in the absence of E_w to $[(\bar{E}_p + \bar{E}_w) \times \bar{B}]/B^2$ in the presence of E_w . However,

$$\bar{V}_e = (\bar{E}_w \times \bar{B})/B^2 = [(\bar{V}_i \times \bar{B}) \times \bar{B}]/B^2 = \bar{V}_i, \quad (2)$$

and hence E_w does not really contribute to the generation of a current; and this is the basis for ignoring, in the earlier years, the effect of a height-invariant wind on the EEJ. By early 1970's the height structures of winds in the lower thermosphere have become known better and the presence of large vertical shears in the zonal and meridional winds became widely recognized both observationally and theoretically.

The effects of such height-varying winds on both the electric fields and currents turn out to be nonnegligible, as detailed in the following sections of this paper. It may be noted here that even a height-invariant wind within the EEJ gives rise to an additional polarization electric field E_w , even though it does not

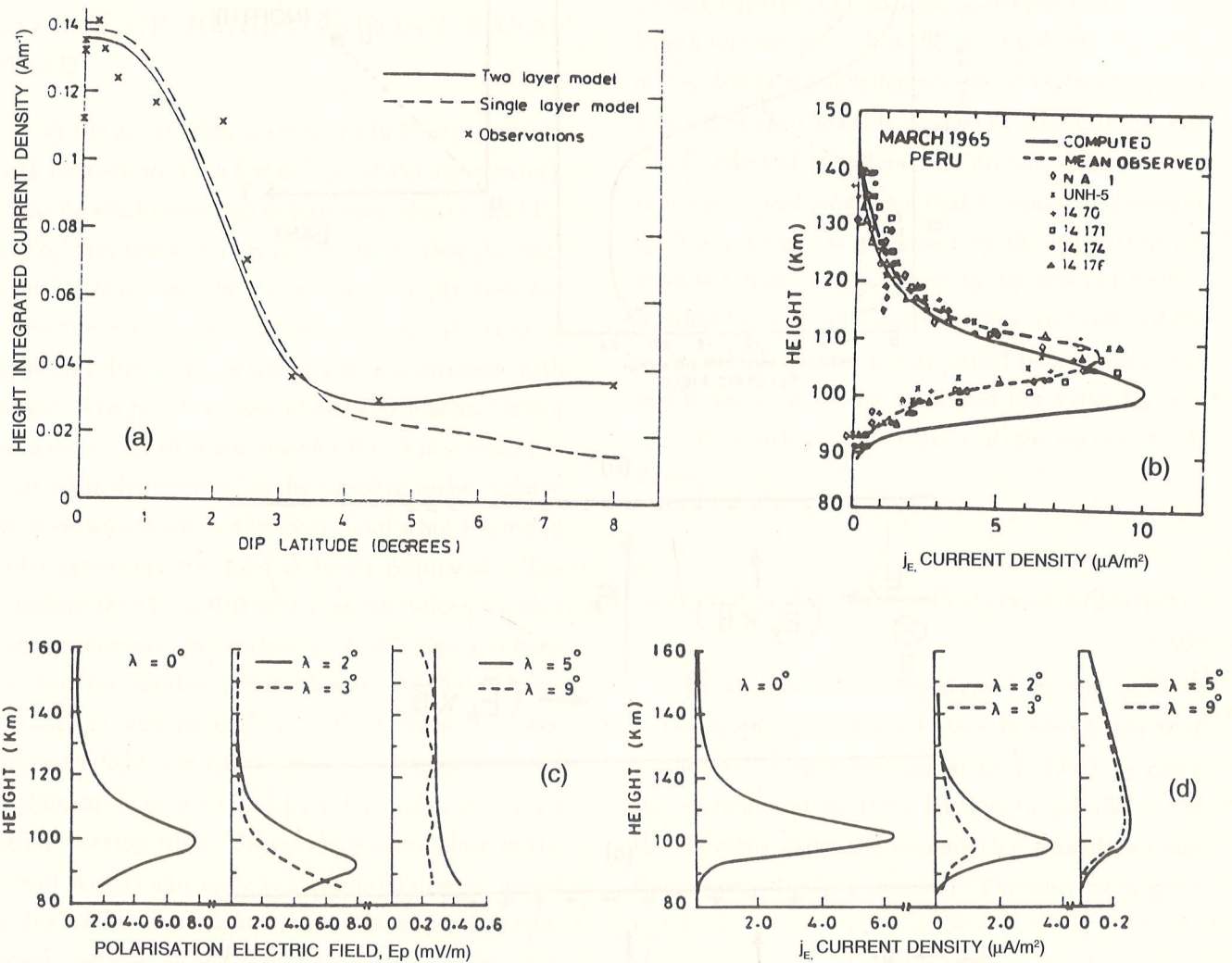


Figure 1. (a) Computed and observed latitude structures of the total current in the equatorial electrojet (from Stening, 1985); (b) computed and observed height structures of the current density in the EEJ at the dip equator (from Richmond, 1973); (c) the computed structures of polarization electric field E_p at different geomagnetic latitudes λ generated by a 0.3 mV/m eastward electric field E_y and (d) computed height structures of current densities corresponding to the E_p fields in (c). Note the discrepancy between the computed and observed heights of maximum current density in (b).

(a) Estruturas latitudinais calculadas e observadas da corrente total no Eletrojoato Equatorial (de Stening, 1985); (b) estrutura vertical calculada e observada da densidade de corrente no Eletrojoato Equatorial no equador dip (de Richmond, 1973); (c) estruturas calculadas do campo elétrico de polarização E_p em várias latitudes geomagnéticas λ causadas por um campo elétrico E_y de oeste para leste de 0,3 mV/m e (d) estrutura vertical calculada para densidade de correntes correspondentes ao campo elétrico E_p de (c). Notar a discrepância entre as alturas calculadas e observadas de máxima densidade de corrente em (b).

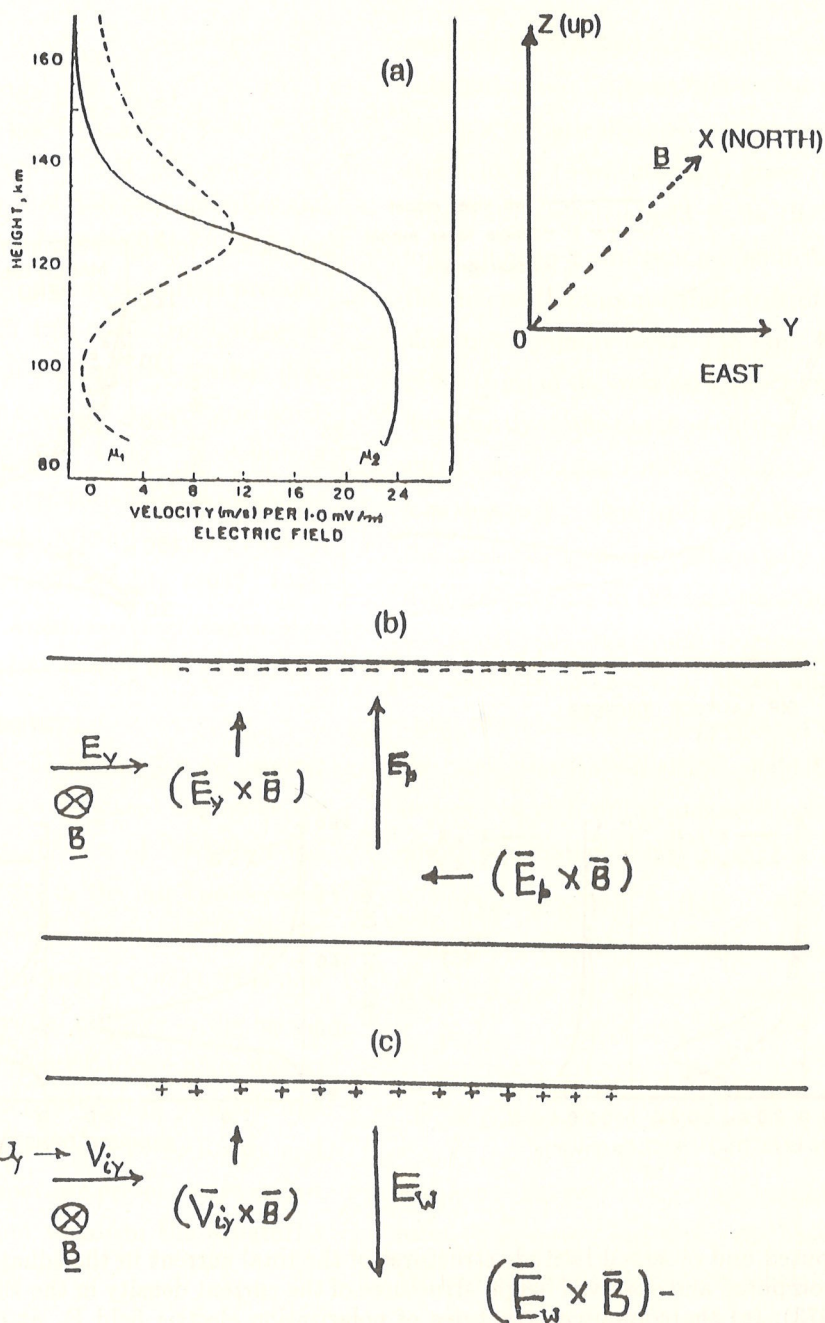


Figure 2. (a) Differential Pedersen drift velocity (μ_1) of ions relative to electrons and differential Hall drift velocity of electrons relative to ions in the presence of a 1.0 mV/m electric field at the magnetic equator. (b) Schematic of a vertical polarization electric field E_p generated by an eastward electric field E_y at the magnetic equator. (c) Schematic explanation of how an eastward wind U_y causes an eastward ion drift V_{iy} which in turn gives rise to a polarization electric field $\bar{E}_w = \bar{V}_{iy} \times \bar{B} \approx \bar{U}_y \times \bar{B}$.

(a) Velocidade de deriva Pedersen diferencial (μ_1) de íons com relação a elétrons e velocidade de deriva Hall diferencial de elétrons com relação a íons na presença de um campo elétrico de 1mV/m no equador magnético. (b) Esquema de um campo elétrico de polarização vertical E_p gerado por um campo elétrico oeste-leste E_y no equador magnético. (c) Esquema que mostra como um vento oeste-leste U_y cria uma velocidades de deriva de íons para leste V_{iy} que, por sua vez gera um campo de polarização $\bar{E}_w = \bar{V}_{iy} \times \bar{B} \approx \bar{U}_y \times \bar{B}$.

generate an additional current; and this electric field is relevant for some processes in the EEJ.

EFFECT OF HEIGHT-VARYING ZONAL WIND

If the zonal wind is changing in height (but not with latitude within a few degrees of the dip equator), then the wind-generated polarization electric field E_w in Fig. 2(c) gets partially discharged so that the east-west electron velocity V_e in equation (2) does not equal the ion velocity V_i , and consequently, there is a current due to E_w which exhibits a variation with height. The physical basis of the above behavior can be understood with reference to Fig. 3 in which $e_s = U_s B$ is the dynamo emf in the "source" region volume element within which the local zonal wind-generated polarization electric field is being estimated. The magnetic field lines B, B enclosing the "source" region volume element also enclose a "load" region volume element (at another location) with the Pedersen resistance r_L and an emf $e_L = U_L B$. Because of the magnetic field line curvature, e_s and e_L are located at different heights so that $U_s \neq U_L$ and $e_s \neq e_L$ for a height-varying wind. Current flow takes place in the circuit ABCD and there is a potential drop e_r across r_s due to this current; and the resultant potential difference between A and D in this case is $e_w = -(e_s - e_r)$, unlike the case of $e_w = e_s$ for $U_s = U_L$ considered in Fig. 2(c). When all the volume elements connected together by the same (highly conducting) magnetic field lines are considered with their differing values of emf's and resistances, the general expression for the wind-generated polarization electric field E_w in any volume element in the EEJ is given by (see Reddy and Devasia, 1981, for details and sign conventions):

$$e_w = e_s + e_r = -\left(\int e_m \sigma_1 ds\right)/(\sigma_1 ds), \quad (3)$$

with integration done along the whole magnetic flux tube length having significant Pedersen conductivity σ_1 . In general, the integration can be terminated

at 80 km level where σ_1 becomes very small even at noontime. If we apply the above methodology, including equation (3), to volume elements with a unit length for each side, then the potential differences e_w and e_r across any side length can be replaced by corresponding electric fields E_w and E_r respectively. The simple physical considerations presented in this section lead to the conclusion that the east-west current j_w at any height as generated by the height-varying wind is a Hall current driven by E_r and not by E_w , because E_r is the difference between the value of $E_w = -e_s$ which would have prevailed in the absence of height variation of the wind and the value $E_w = -e_s + E_r$ which prevails with a height-varying wind. Hence,

$$j_w(z) = \sigma_2(z) E_r(z) = \sigma_2(z) [e_s - (e_m \sigma_1 ds)] / (\sigma_1 ds). \quad (4)$$

In addition, a wind-generated current j_1 flows in the magnetic meridional plane in such a way that in the path length orthogonal to \bar{B} the ions carry the current and in the path length parallel to \bar{B} the electrons carry the current (see Anandarao and Raghavarao, 1987, for details). This current is given by:

$$j_1(z) = \sigma_1(z) E_r(z). \quad (5)$$

TWO APPROACHES

Two different approaches have been used in treating the effects of height-varying winds on the EEJ: (i) solving the differential equations relating the currents and electric fields to the winds and conductivities in the EEJ, and (ii) the method of equivalent circuit analysis. Richmond (1973), Fambitakoye et al. (1976), Anandarao and Raghavarao (1987) used the first approach, while Kato (1973), Reddy and Devasia (1978, 1981), and Stening (1985) used the second approach. Both approaches are expected to give the same results, but no explicit treatment of this equiv-

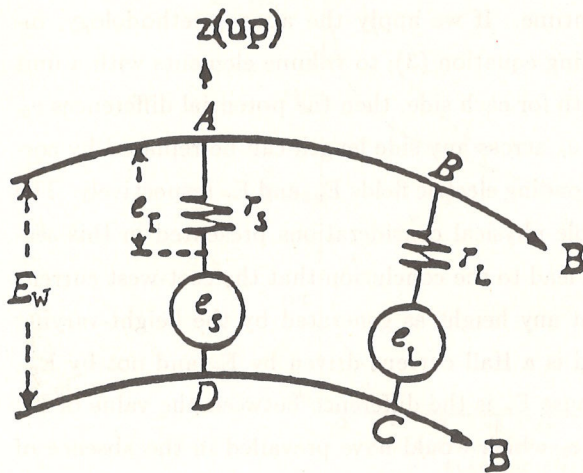


Figure 3. Equivalent circuit method of treating the electric field generation process by a height-varying wind in the EEJ. See text for detailed explanation (from Reddy and Devasia, 1978).

Método do circuito equivalente para tratar o processo de criação de um campo elétrico por um vento que varia com altura no Eletrojato. Ver texto (de Reddy e Devasia, 1978).

alence has been attempted.

As is to be expected, different researchers have emphasized different aspects of the wind effects, thus providing a very good view of how the altitude and latitude structures of the EEJ are affected by the local interactions of the winds in the EEJ. Sample results from the paper of the above researchers are shown in Fig. 4 to provide a good perspective view of the wind effects on the EEJ.

Fig. 4 shows how a height-varying zonal wind U_y (+ve eastward) in Fig. 4a generates a current which alters the height structure of the electrojet current at $\lambda = 0^\circ$ and $\lambda = 3^\circ$ (λ being geomagnetic latitude) as shown in Fig. 4b,c. The latitude variations of the total height-integrated current intensity due to the eastward electric field E_y of global wind dynamo origin and due to the local effect of U_y in Fig. 4a are shown in Fig. 4d. Fig. 4 also shows the results of earlier calculations done by Richmond (1973) along with some rocket-borne magnetometer measurements of current

profiles. This figure shows that (i) the wind-generated current, either in terms of current density at any altitude or the height-integrated current intensity, is rather small within $\pm 2^\circ$ of the magnetic equator in relation to the E_y -generated current, and (ii) the wind-generated currents can exceed or even dominate the E_y -generated current at $\lambda \geq 3^\circ$.

The situation is distinctly different with regard to the polarization electric fields generated locally by height-varying winds. Fig. 5a shows three typical wind profiles and Figs. 5b and 5c show the height structures of the electric fields at different latitudes as generated by U-3 and U-8 profiles, respectively. In each case, $e_s = U_s B$ is the local dynamo electric field due to the local wind U_s , while E'_p which is the same as E_w in equation (3), is the polarization electric field generated by e_s in the presence of the short-circuiting effect of the Pedersen currents flowing in all the volume elements connected by the magnetic field lines to the volume element with e_s (as shown in Fig. 3). In the absence of this short-circuiting effect, E'_p would have equalled e_s . The electric field E_r is the difference between e_s and E'_p (see equation (3)) and it represents the potential drop per unit length in the volume element with U_s and e_s due to the current driven through it by the combined action of all the emf's e_m in all the volume elements contained within the same magnetic flux tube. Figs. 5b,c show that the wind-generated electric field E'_p (i.e., E_w in equation (3)) can have magnitudes which are comparable to a substantial fraction of the E_y -generated field E_p (Fig. 1c) at some altitudes. Moreover, it can have steeper gradients than E_p at some altitudes; and most importantly, it can reverse direction (upward to downward or vice versa) more than once within the EEJ altitude range, depending upon the height structure of the wind. The reality of such large variations of E_w with height, including the direction reversals, has been borne out by the VHF radar observations at Thumba near Trivandrum (Reddy, 1989) in India and at Jicamarca in Peru (Kudeki et al., 1987). An

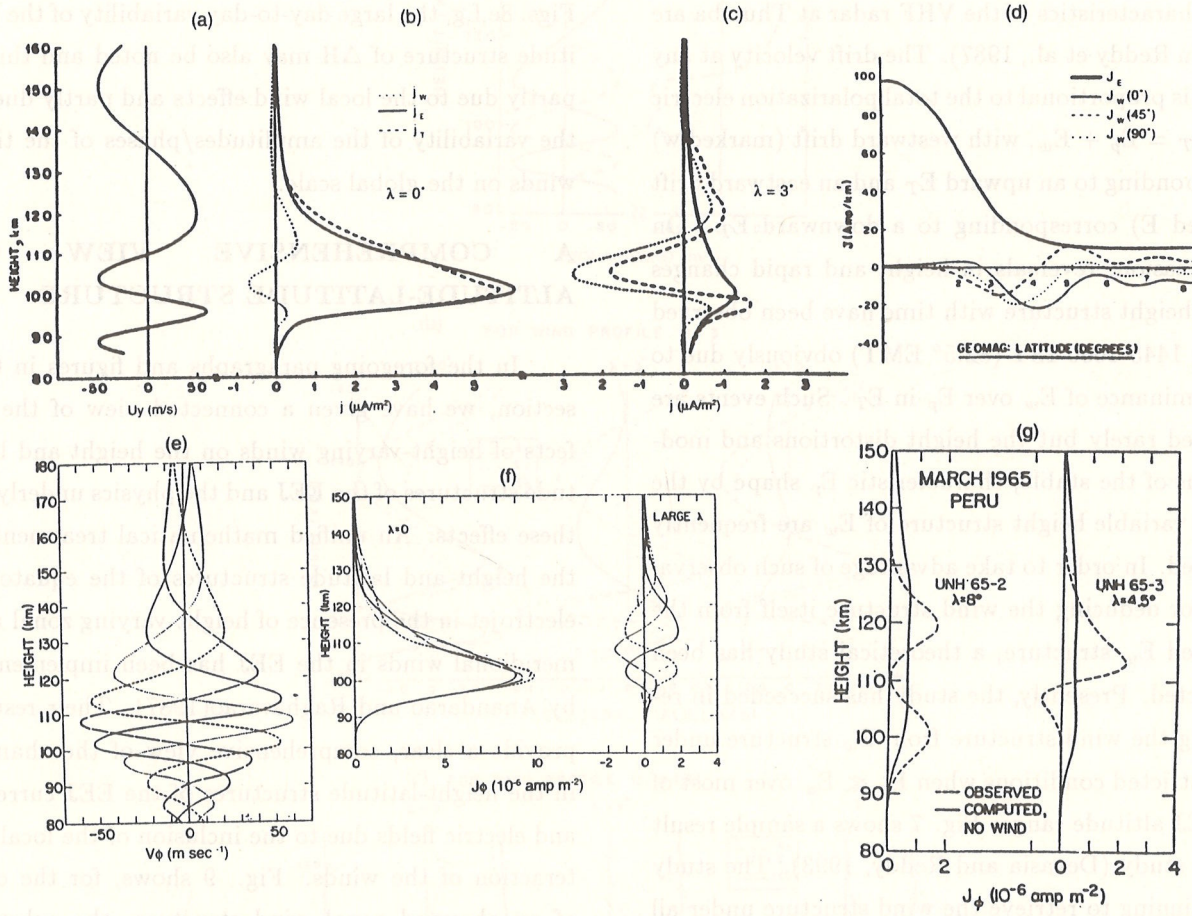


Figure 4. (a) A model profile of U_y , east-west wind; (b) the profile of east-west current (j_w) generated by the wind in (a) (dotted line) - the broken line gives the current profile (j_E) due to a 0.3 mV/m eastward electric field E_y and the solid line is the sum of j_w and j_E at 0° gm latitude; (c) same as (b) except for $\lambda = 3^\circ$; (d) latitude variations of total height-integrated currents J_E and J_w for different wind models similar to that in (a); (e) and (f): similar profiles of wind and computed currents as taken from Richmond (1973); (g) Currents as measured with rocket-borne magnetometers (from Richmond, 1973).

(a) Um modelo de perfil de U_y , vento leste-oeste; (b) o perfil de corrente leste-oeste (j_w) gerada pelo vento em (a) (linha pontilhada) - a linha tracejada mostra o perfil de corrente (j_E) devido a um campo elétrico para leste de 0.3 mV/m E_y e a linha sólida é a soma de j_w e j_E em latitude geomagnética de 0° ; (c) o mesmo que (b) exceto para $\lambda = 3^\circ$; (d) variações latitudinais das correntes elétricas integradas J_E e J_w para diferentes modelos de ventos semelhantes ao caso (a); (e) e (f): perfis semelhantes (de ventos e correntes calculadas) aos de Richmond, 1973; (g) correntes medidas com magnetômetros instalados em foguetes (de Richmond, 1973).

observation of a dramatic event is shown in Fig. 6. In Fig. 6a, the line-of-sight drift velocity of the 2.75 meter size irregularities in the EEJ as measured by a pulse coherent backscatter radar of 54.95! MHz (at an elevation angle of 60°) is shown for various times (The characteristics of the VHF radar at Thumba are given in Reddy et al., 1987). The drift velocity at any height is proportional to the total polarization electric field $E_T = E_p + E_w$, with westward drift (marked w) corresponding to an upward E_T and an eastward drift (marked E) corresponding to a downward E_T . On this occasion, reversals in height and rapid changes in the height structure with time have been observed during 1445-1600 1ST (82.5° EMT) obviously due to the dominance of E_w over E_p in E_T . Such events are observed rarely but the height distortions and modulations of the stable, characteristic E_p shape by the highly variable height structure of E_w are frequently observed. In order to take advantage of such observations for deducing the wind structure itself from the observed E_w structure, a theoretical study has been conducted. Presently, the study has succeeded in retrieving the wind structure from E_w structure under the restricted conditions when $E_p \ll E_w$ over most of the EEJ altitude range: Fig. 7 shows a sample result of this study (Devasia and Reddy, 1993). The study is continuing to retrieve the wind structure under all conditions irrespective of the relative magnitudes of E_p and E_w .

LATITUDE STRUCTURE

Fig. 8 depicts how the latitude structure of the EEJ current-intensity and correspondingly, the ground-level magnetic field component H are altered by the action of height-varying winds. The computed results are shown for the two model wind profiles U-1, U-3 shown in Fig. 5a. It can be seen that the effect of the winds is negligible within $\pm 2^\circ$ of the dip equator, but it can be very large beyond $\pm 3^\circ$ gm. latitude. Again, the reality of such modulations in the latitude structure is borne out by excellent observations with

a latitudinal chain of ground-level magnetometers, as shown in Figs. 8f,g. The occurrence of the double-humped structures in the ΔH variation with latitude can be seen at 12:30 to 14:30 hours on September 22, 1969 and at 11:30-12:30 hours on July 15, 1969. In Figs. 8e,f,g, the large day-to-day variability of the latitude structure of ΔH may also be noted and this is partly due to the local wind effects and partly due to the variability of the amplitudes/phases of the tidal winds on the global scale.

A COMPREHENSIVE VIEW OF ALTITUDE-LATITUDE STRUCTURE

In the foregoing paragraphs and figures in this section, we have given a connected view of the effects of height-varying winds on the height and latitude structures of the EEJ and the physics underlying these effects. An unified mathematical treatment of the height and latitude structures of the equatorial electrojet in the presence of height-varying zonal and meridional winds in the EEJ has been implemented by Anandarao and Raghavarao(1987). Their results provide a clear, comprehensive view of the changes in the height-latitude structures of the EEJ currents and electric fields due to the inclusion of the local interaction of the winds. Fig. 9 shows, for the case of an observed zonal wind structure, the substantial differences in the height-latitude structures of the EEJ electric fields, currents and ground-level magnetic fields with the exclusion and inclusion of the observed wind structure. The changes in the current, electric field, ΔH , ΔZ are found to be rather small within $\pm 2^\circ$ of dip equator, but large changes in the above parameters are present due to the effect of the height-varying zonal wind. The inclusion of the height-varying meridional wind (as observed at Thumba) seems to cause significantly smaller (but nonnegligible) effects than the effects of the zonal wind (shown in Fig. 9a). This can be understood qualitatively in terms of the much smaller efficiency of the meridional wind in generating the dynamo and

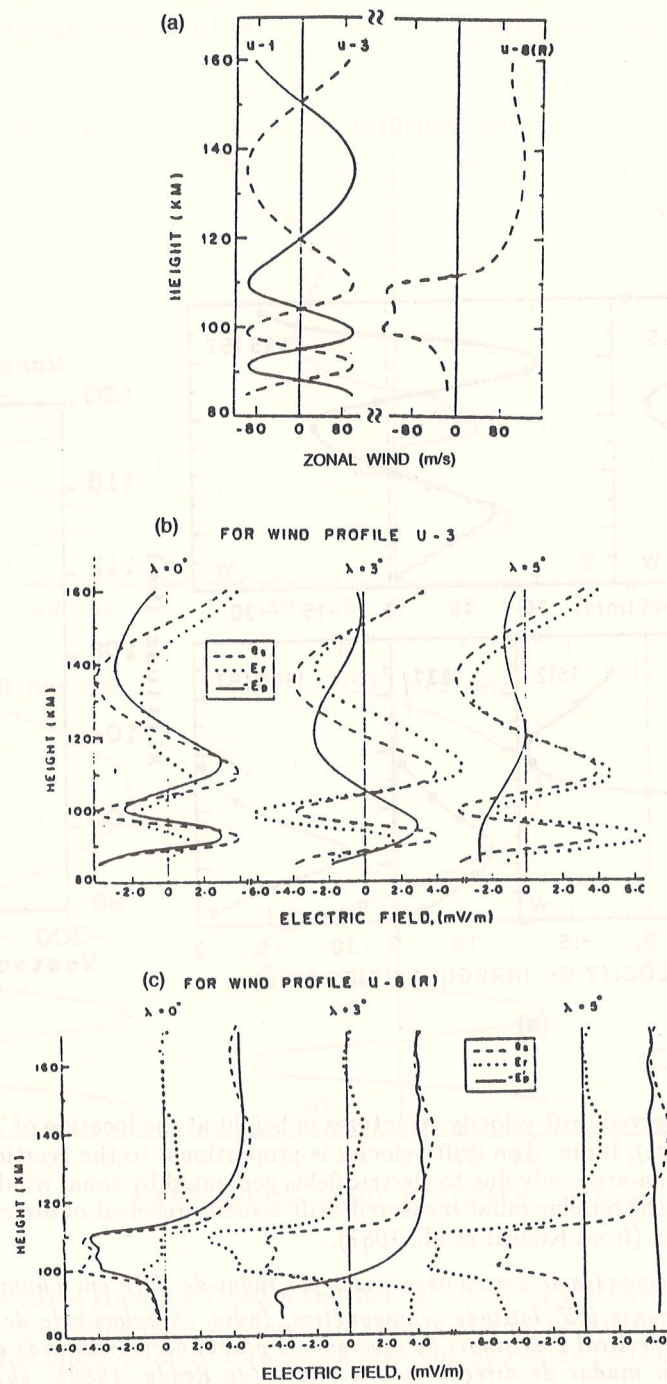


Figure 5. (a) Model wind profiles used for computing wind-generated electric fields and currents; (b), (c): electric fields generated by the wind profiles shown in (a). E'_p is the same as E_w in equation (3) and Fig. 3. See text for details (from Reddy and Devasia, 1981).

(a) Modelos de perfis de ventos usados para calcular os campos elétricos gerados e correntes; (b), (c): campos elétricos gerados pelos perfis de ventos mostrados em (a). E'_p é igual a E_w na equação (3) e Fig. 3. Ver texto para detalhes (de Reddy e Devasia, 1981).

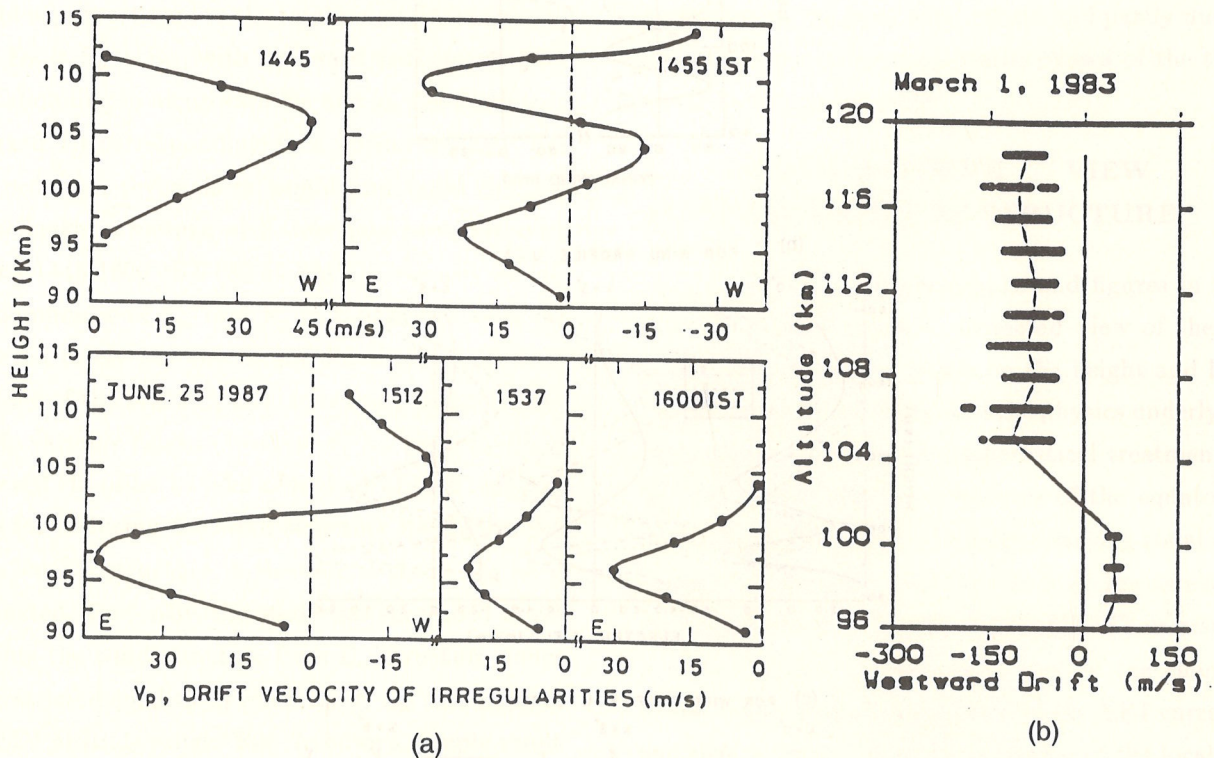


Figure 6. (a) VHF radar-observed drift velocity structures in height at the location of Thumba near Trivandrum (8.5°N , 77°E ; $\sim 0.5^{\circ}$ s gm. lat.), India. The drift velocity is proportional to the (vertical) polarization field and the sign reversals of velocity can arise only due to electric fields generated by zonal winds changing direction with altitude (from Reddy, 1989). (b) Similar radar-measured drift velocity reversal of direction as observed with the high power radar at Jicamarca (from Kudeki et al., 1987).

(a) Estruturas verticais de velocidades de deriva observadas por radar de VHF em Thumba próximo a Trivandrum ($8,5^{\circ}\text{N}$, 77°E); aproximadamente $0,5^{\circ}$ latitude geomagnética, Índia. A velocidade de deriva é proporcional ao campo elétrico de polarização vertical e os sinais de reversão só podem ocorrer através de outros campos elétricos gerados por ventos que podem mudar de direção com a altura (de Reddy, 1989). (b) Mudança de direção de velocidades de deriva observadas pelo radar de Jicamarca (de Kudeki et al., 1987).

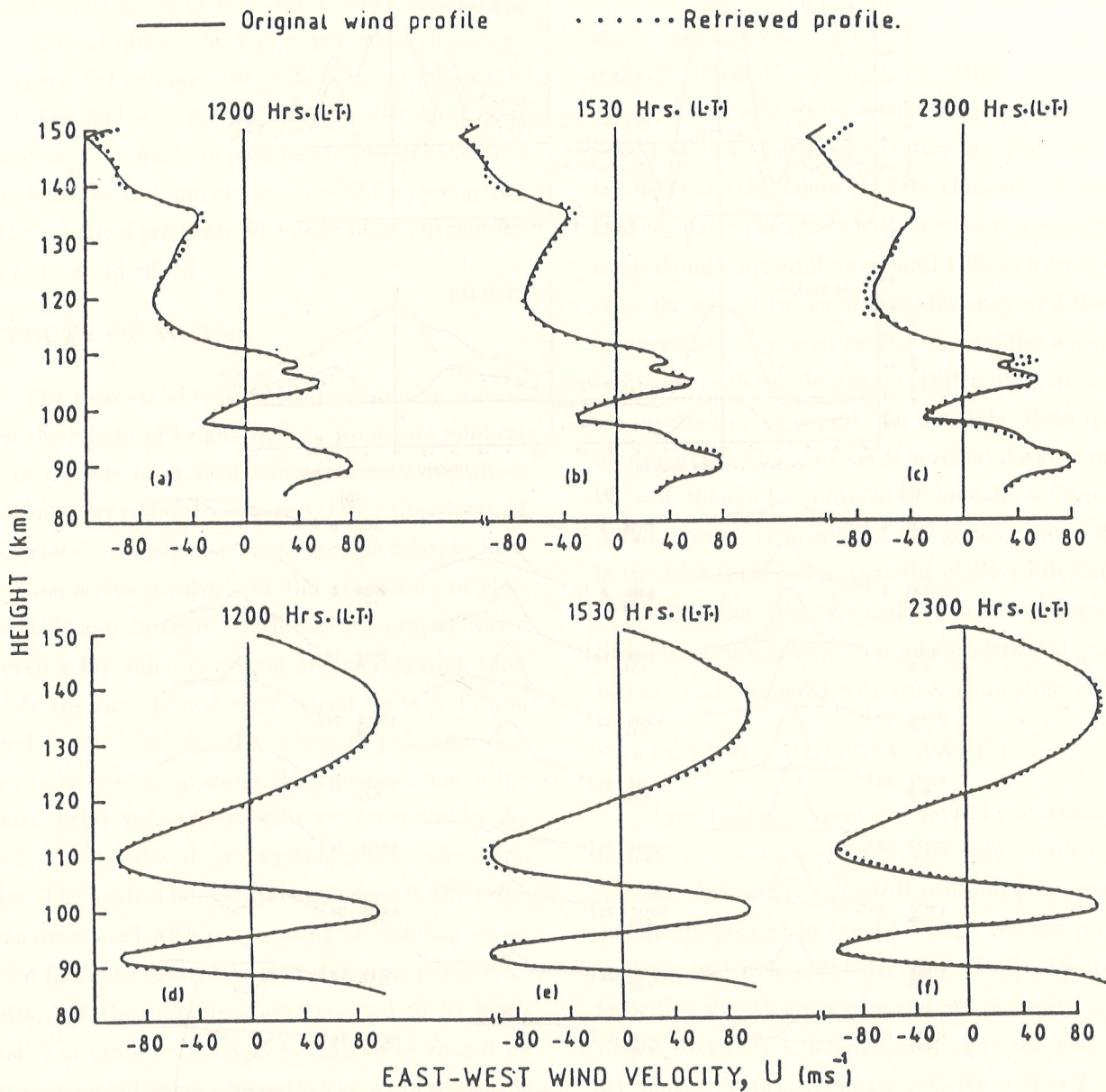


Figure 7. Results of a simulation study by Devasia and Reddy (1993) for the retrieval of height-varying winds from the height-varying electric fields (E_w) produced by them. The input wind profiles (solid lines) and the retrieved wind profiles (dotted lines) obtained through an inversion procedure (which uses assumed conductivity profiles at 12:00, 15:30 and 23:00 LT) are shown.

(a) Resultados de uma simulação teórica de Devasia e Reddy (1993) para deduzir os ventos e sua variação com altura a partir dos campos elétricos (E_w). São mostrados os perfis de entrada dos ventos (linhas sólidas) e os perfis de ventos deduzidos (linhas pontilhadas) obtidos por inversão (que assume perfis de condutividade às 12:00, 15:30 e 23:00 horas local).

Effects of Winds and Waves on the Equatorial Electrojet

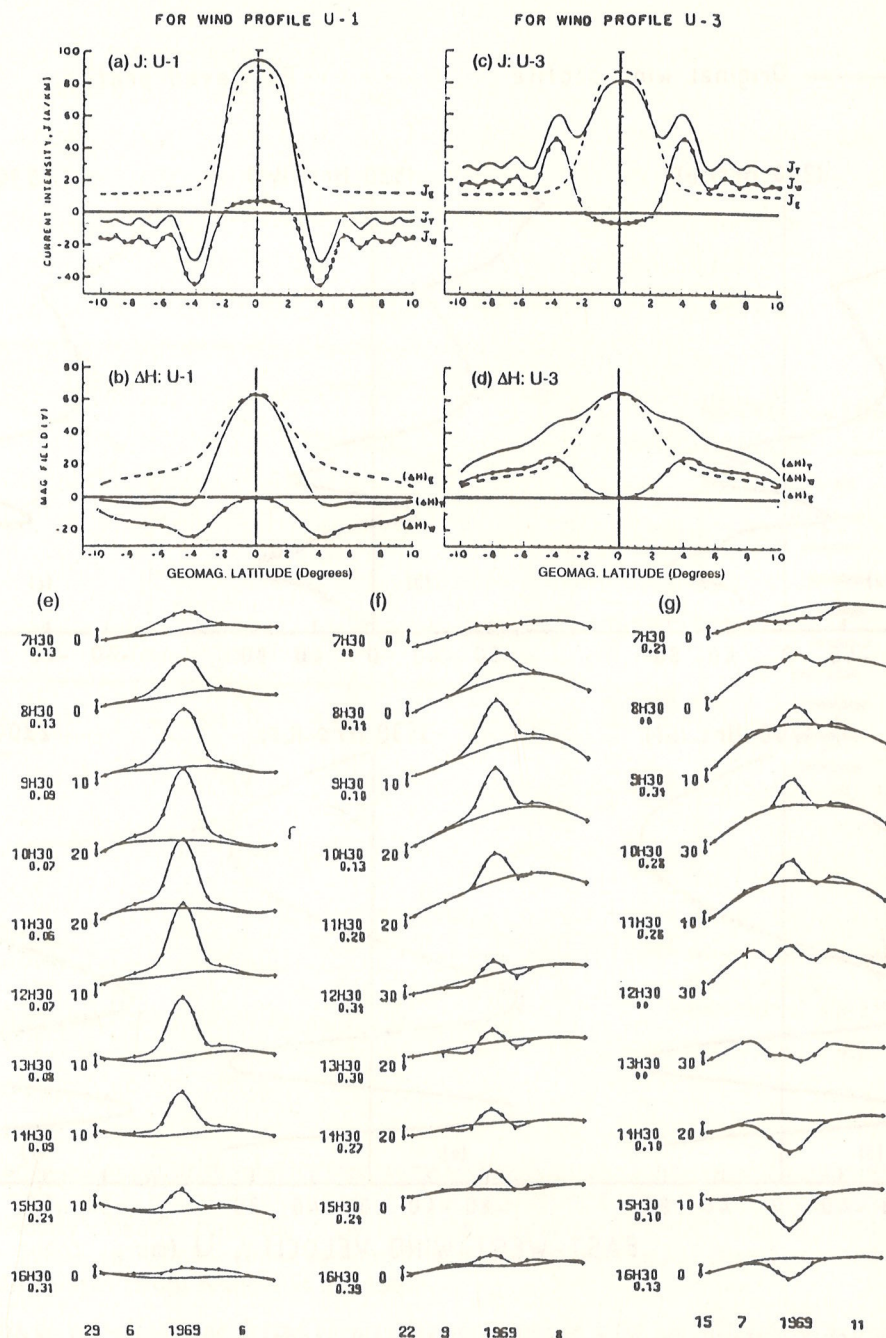


Figure 8. (a), (b), (c), (d): Latitude structures of the EEJ current intensity with and without the wind effects, for the case of U-1 and U-3 profiles in Fig. 5a, and the corresponding latitude structures of ΔH , the ground-level magnetic field perturbations (from Reddy and Devasia, 1981). (e), (f), (g): Latitude structures of ΔH at different local times for three different days. The abscissa represents a latitude range of about 27° with the dip equator near the center. The scale marked corresponds to 10nT and the value near the scale shows the base line value in nT. Date, month, year are shown in each case. There are nine experimental values for each curve corresponding to the nine stations in the latitudinal chain. (from Fambitakoye and Mayaud, 1976).

(a), (b), (c), (d): Estruturas latitudinais das intensidades de corrente no eletrojato com e sem os efeitos de ventos, para os casos dos perfis U-1 e V-3 da Fig. 5a, e as estruturas latitudinais correspondentes de ΔH , as perturbações de superfície do campo magnético (de Reddy e Devasia, 1981). (e), (f), (g): Estruturas latitudinais de ΔH em diferentes horários para três dias diferentes. A abscissa representa um intervalo de latitude de 27° , com o equador dip ao centro. A escala marcada corresponde a 10nT e o valor próximo à escala mostra o valor da linha base em nT. Em cada caso mostra-se a data, o mês e o ano. Há nove valores experimentais para cada curva correspondentes às nove estações de distribuição latitudinal (de Fambitakoye e Mayaud, 1976).

polarization electric fields in the vicinity of the magnetic equator due to the very small values of the geomagnetic field component orthogonal to the meridional flow and due to the much smaller horizontal gradients of the medium parameters (such as the electron densities and ion, electron mobilities) compared to their vertical gradients which are more relevant for the zonal wind effects.

EFFECTS OF WAVES

The theoretical treatments presented in section 3 on the effects of height-varying winds are applicable to the effects of such atmospheric waves, whose horizontal wavelengths are very large (hundreds of kilometers) and whose periods are much larger than the time scales involved for the generation of electric fields and currents. Both acoustic-gravity waves of even a few minutes period and propagating tides satisfy the time period requirement quite well; and therefore, the theoretical treatments presented earlier can be used to quantify the time evolution of the electric fields and currents that are generated by the winds associated with propagating gravity waves and tides. The neutral temperature and density perturbations associated with propagating or standing waves in the EEJ also contribute to the changes in the electrojet, but these changes are expected to be much smaller in most circumstances than those caused by wave-associated winds. Nevertheless, a full treatment of this problem in relation to the EEJ changes may be very useful. While the tidal winds have very large scale for their horizontal variations to justify the neglect of wind-generated gradients in the horizontal direction, the same is not true of gravity waves which may have horizontal wavelengths as small as 50 km. The effects of wave-generated gradients in the EEJ parameters in the zonal and meridional directions become significant for such waves and only a three-dimensional treatment for different wave vector directions can give quantitatively reliable results on the wave effects in the EEJ.

The wave-generated electric fields, ion convergences and currents in the EEJ were treated theoretically in different ways by Kato (1973), Anandarao et al. (1977) and Prakash and Pandey (1985). All these papers predict the generation of significant electric fields and they show that the efficiency of electric field generation increases with increasing values of the vertical and horizontal wavelengths of the wave. However, the actual values of this efficiency and the ion convergences generated by the waves differ widely as estimated in the above papers. Different assumptions are involved in all papers: for example, Kato makes his calculations for the case of horizontal wavenumber $kH = 0$, though his formulation includes a finite kH . A full rigorous treatment of the gravity wave effects in the EEJ is needed so that the observed deviations of the EEJ from the "normal" structure expected in the absence of wave effects can be understood quantitatively and compared with other competing effects.

EFFECTS ON PLASMA WAVES

Type I plasma waves generated by a two-stream instability process and type II waves generated by a gradient drift or $(\bar{E} \times \bar{B})$ drift instability process are commonly present in the EEJ (e.g. see the reviews by Fejer and Kelley, 1980; Farley, 1985). The phase velocities of both types of waves are measured by coherent backscatter radars operating in the VHF and HF ranges. $V_p^I(\theta)$, the phase velocity of type I waves and $V_p^{II}(\theta)$ of type II waves in the magnetic east-west plane are given by (eg., see Broche et al., 1978; Cohen and Hooke, 1978; Ravindran and Reddy, 1993):

$$V_p^I(\theta) \approx (V_{ey} - V_{iy}) \cos\theta / (1 + \alpha). \quad (6)$$

$$V_p^{II}(\theta) \approx [C_E(E_y/B) + C_w U_y] \cos\theta. \quad (7)$$

In the above equations, θ is elevation angle, V_{ey} (V_{iy}) is the electron (ion) drift velocity, U_y is the wind velocity and E_y is the electrostatic field, all in the magnetic east-west direction, B is the geomagnetic field, and $\alpha = \rho_i / \rho_e$, with ρ_i and ρ_e being the

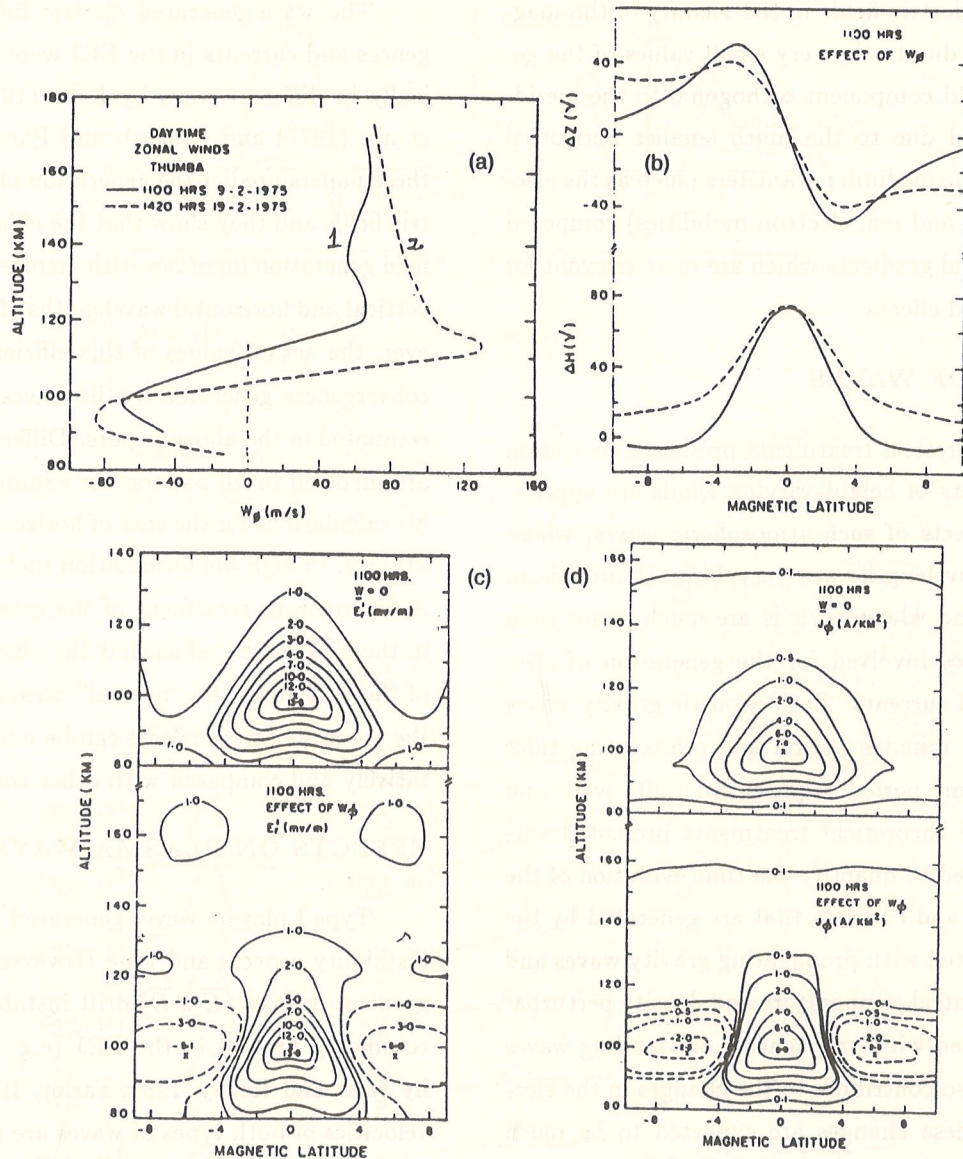


Figure 9. (a) Zonal winds measured at Thumba (8.5°N , 77°E) in India at 11:00 LT and 14:20 LT. $W_\varphi - 1$ is W_φ at 11:00 LT. (b) Latitude structures of the computed ground-level magnetic field perturbations ΔZ , ΔH caused by j_φ shown in (d), with $W_\varphi - 1$ included (solid lines) and not included (dashed lines). (c) Altitude-latitude distribution of the computed E'_r , the vertical electric field, in the magnetic meridional plane: top panel shows generated by 0.5 mV/m eastward electric field (E_y) excluding the zonal wind 1 in (a) and bottom panel shows E'_r with the inclusion of zonal wind 1 in addition to E_y . Positive E'_r is upward (solid line). (d) The altitude-latitude structure of the computed east-west current density j_φ excluding $W_\varphi - 1$ (top panel) and including (bottom panel). Positive j_φ is eastward (solid lines). The entire figure is from Anandarao and Raghvarao (1987).

(a) Ventos zonais medidos em Thumba (8.5°N , 77°E), Índia, às 11:00 e 14:20 horas locais. $W_\varphi - 1$ é W_φ às 11 h. (b) Estruturas latitudinais das perturbações magnéticas de superfície ΔZ e ΔH causadas por j_φ mostradas em (d), com $W_\varphi - 1$ incluído (linhas sólidas) e não-incluído (linhas tracejadas). (c) Distribuição com latitude e altitude dos campos elétricos E'_r , verticais, no plano magnético meridional: painel superior mostra resultado de um campo elétrico de 0.5 mV/m oeste-leste (E_y) sem o vento zonal 1 em (a) e o painel inferior mostra E'_r incluindo o efeito do vento zonal. E'_r positivo é para cima (linha sólida). (d) Estrutura de latitude-altitude da corrente elétrica calculada de leste a oeste j_φ sem $W_\varphi - 1$ (painel superior) e com W_φ (painel inferior). Corrente j_φ positiva é de oeste para leste (linha sólida). Figura de Anandarao and Raghvarao (1987).

ratios of the collision frequency to the gyrofrequency of the ions and electrons respectively. $C_E = \rho_i / (1 + \alpha)^2$ and $C_w = \alpha \rho_i^2 / [(1 + \alpha)(1 + \rho_i^2)]$. At 100 km altitude, $C_E \sim 25$, $C_w \sim 0.2$, $\alpha \sim 0.1$. $E_y/B \approx 30$ m/s for $E_y = 1.0$ mV/m and $B = 0.33$ Gauss. $V_{ey} \sim (E_y/B)[\rho_i/(1 + \alpha)]$ and $V_{iy} \sim U_y$ at 100 km height. From the above numbers, we can see that $V_p^I(\theta)$ varies linearly and substantially with U_y for a given V_{ey} condition; and U_y can indeed be inferred from observed $V_p^I(\theta)$ values if we have an independent estimate of V_{ey} , or $V_p^I(\theta)$ measurements for different θ values. An example of such inference of U_y from radar-measured V_p^I values at different zenith angles is shown in Fig. 10. With appropriately planned radar measurements, the zonal winds in a considerable range of EEJ can be deduced whenever type I plasma waves are present in the EEJ. In contrast, V_p^{II} is very little affected by U_y at 100 km level due to the small value of C_w at this height. However, at lower altitudes of 95 km and below, U_y has considerable effect on V_p^{II} due to increasing values of C_w with decreasing altitude. In Fig. 11, (a) and (b) show the lunar tide-related wind effects on the EEJ as observed with ground-level magnetometer and with a VHF radar (in terms of the radar Doppler frequency and signal strength changes). While the radar observations show large perturbations in \bar{f}_D and V around noon on May 12, 1975 (Fig. 11a) and in the afternoon on February 23, 1978 (Fig. 11b), the corresponding perturbations in ΔF are barely discernable. This behavior can be understood in terms of the schematic explanation in Fig. 11c: the EEJ has suffered large changes in its bottomside and these are measured by the radar, while the height-integrated current intensity undergoes very small changes with the result that the changes in ΔF are rather small (see Reddy et al., 1980 for details).

CONCLUDING REMARKS

As emphasized in the author's earlier reviews on the equatorial electrojet, the EEJ is a multifaceted phenomenon subject to the influences of several basic processes in the ionosphere-thermosphere-magnetosphere system. Some of the influencing processes are very distant from the EEJ location such as the enhanced magnetospheric convection electric fields which significantly perturb the EEJ. In contrast, the effects of winds and waves dealt with in this paper concern the local processes within the EEJ. The question then is: what effects do these local wind-generated electric fields have on the ionospheric medium outside the EEJ? An investigation of this question is yet to be taken up. The magnetometer and radar studies to date have given only a glimpse of the substantial effects of the height-varying winds on the structure of the EEJ. A satisfactory quantitative characterization of these effects has yet to be accomplished through the relevant observations. The planned systematic effort of coordinated, global observations during the IEEY will hopefully advance such characterization. Most importantly, the retrieval of the height-varying winds in the EEJ from the height-varying electric fields generated by such winds will be a decisive advance towards the understanding of the lower thermospheric winds near the magnetic equator. Hopefully, a successful method will be evolved for this purpose.

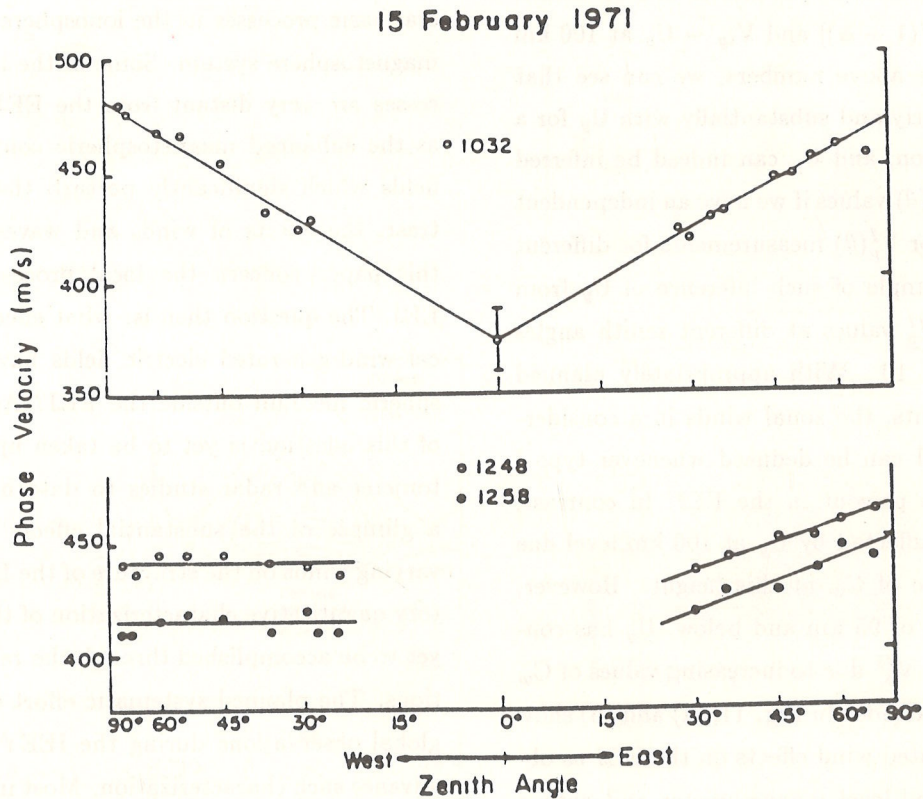


Figure 10. Jicamarca (Peru) radar observations of type I plasma wave phase velocities in the EEJ at different zenith angles. In the upper panel, the increase of phase velocity with increasing zenith angle (θ), linear with $\sin \theta$, is attributed to the presence of ~ 105 m/s zonal wind at 10:32 LT. In contrast, the lower panel indicates the absence of such a wind to the west of the zenith and the presence of a much smaller wind to the east of the zenith, at 12:48 and 12:58 LT (from Balsley et al., 1976).

(a) Velocidades de fase de ondas de plasma do tipo I, observadas pelo radar de Jicamarca no eletrojato a vários ângulos zenitais. No painel superior, o aumento de velocidade de fase com ângulo zenital θ , linearmente com seu θ , é atribuído à presença de um vento zonal de 105 m/s às 10:32 horas (local). No painel inferior, ao contrário, não ocorre a presença de vento a oeste e apenas um pequeno vento a leste do zênite, às 12:48 e 12:58 (de Balsley et al., 1976).

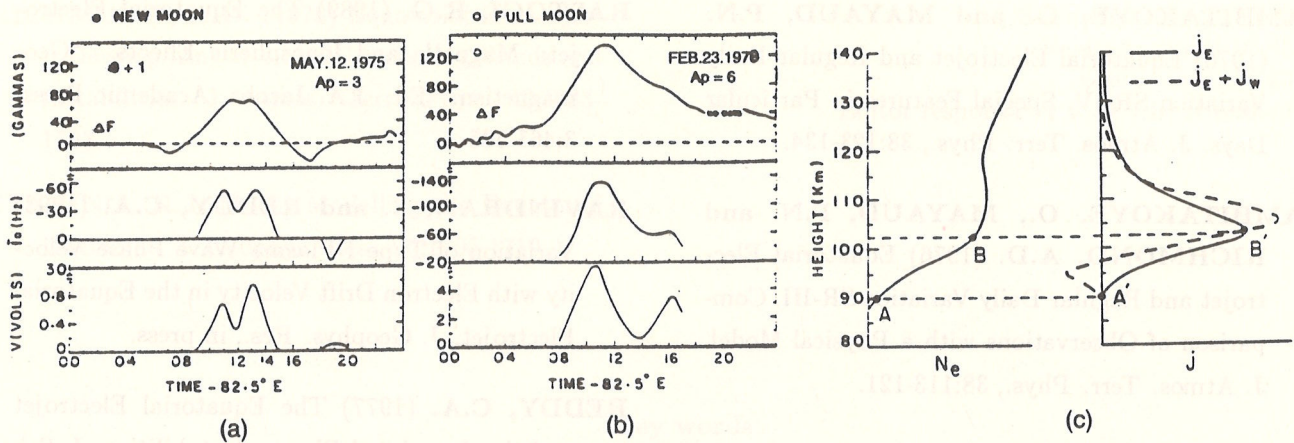


Figure 11. (a),(b): Time variations of ΔF , the ground-level geomagnetic field strength above the nighttime level, the 54.95 MHz backscatter radar Doppler frequency (\bar{f}_D) and radar signal strength (V) at Thumba ($8.5^\circ N$, $77^\circ E$; $0.5^\circ S$ gm. lat.) in India, on two days near New Moon and Full Moon. (c) Schematic of explanation for the barely discernable changes in ΔF at noontime in (a) and around 14 LT in (b) even while large changes are observed in (\bar{f}_D) and (V) (from Reddy et al., 1980).

(a), (b): *Variações temporais de ΔF , a intensidade do campo magnético de superfície acima do valor noturno, e a intensidade do sinal de radar (V) e a frequência Doppler de radar de retroespalhamento em 54,95 MHz (\bar{f}_D) em Thumba ($8.5^\circ N$, $77^\circ E$, $0.5^\circ S$ lat. geom.) na Índia, em dois dias próximos à lua nova e à lua cheia; explicação esquemática para as quase imperceptíveis mudanças em ΔF ao meio-dia (a) e perto de 14:00 horas em (b) ainda que grandes variações sejam observadas em (\bar{f}_D) e (V) (de Reddy et al., 1980).*

ACKNOWLEDGEMENT

The work resulting in this paper has been done during the tenure of the author as a Senior Research Associate of the National Research Council of the U.S.A. The financial support of the NRC, and the warm hospitality of the Planetary Atmospheres Branch are gratefully acknowledged. The author is thankful to Lori Winter for her excellent typing of the paper.

REFERENCES

- ANANDARAO, B.G. and RAGHAVARAO, R. (1987) Structural Changes in the Currents and Fields of the Equatorial Electrojet due to Zonal and Meridional Winds. *J. Geophys. Res.*, 92: 2514-2526.
- ANANDARAO, B.G., RAGHAVARAO, R. and RAGHAVA REDDI, C. (1977) Electric Fields by Gravity Wave Winds in the Equatorial Ionosphere. *J. Geophys. Res.*, 82:1510-1512.
- BALSLEY, B.B., FEJER, B.G. and FARLEY, D.T. (1976) Radar Measurements of Neutral Winds and Temperatures in the Equatorial E Region. *J. Geophys. Res.*, 81:1457-1459.
- BROCHE, P., CROCHET, M. and GAGNEPAIN, J. (1978) Neutral Winds and Phase Velocity of the Instabilities in the Equatorial Electrojet. *J. Geophys. Res.*, 83:1145-1146.
- COHEN, R. and HOOKE, W.H. (1978) Neutral Atmospheric Motions manifested in Radar Echo Doppler Shifts from Two-stream Irregularities in the Equatorial Electrojet. *J. Geophys. Res.*, 83:4791-4797.
- DEVASIA, C.V. and REDDY, C.A. (1993) Retrieval of East-west Wind in the Equatorial Electrojet from the Local Wind-generated Electric Field. *J. Geophys. Res.*, (communicated).

- FAMBITAKOYE, O. and MAYAUD, P.N.** (1976) Equatorial Electrojet and Regular Daily Variation SR-IV. Special Features in Particular Days. *J. Atmos. Terr. Phys.*, 38:123-134.
- FAMBITAKOYE, O., MAYAUD, P.N. and RICHMOND, A.D.** (1976) Equatorial Electrojet and Regular Daily Variation SR-III. Comparison of Observations with a Physical Model. *J. Atmos. Terr. Phys.*, 38:113-121.
- FARLEY, D.T.** (1985) Theory of Equatorial Electrojet Plasma Waves: New Developments and Current Status. *J. Atmos. Terr. Phys.*, 47:729-737.
- FEJER, B.G. and KELLEY, M.C.** (1980) Ionospheric Irregularities. *Reviews of Geophys. and Space Phys.* 18:401-454.
- FORBES, J.M.** (1981) The Equatorial Electrojet. *Rev. Geophys.*, 19:469-504.
- KANE, R.P.** (1976) Geomagnetic Field Variations. *Space Sci. Rev.*, 18:413-540.
- KATO, S.** (1973) Electric Field and Wind Motion at the Magnetic Equator. *J. Geophys. Res.*, 78:757-762.
- KUDEKI, E., FEJER, B.G., FARLEY, D.T. and HANUISE, C.** (1987) The Condor Equatorial Electrojet Campaign: Radar Results. *J. Geophys. Res.*, 92:13,561-13,577.
- MAYAUD, P.N.** (1977) The Equatorial Counter Electrojet-a Review of its Geomagnetic Aspects. *J. Atmos. Terr. Phys.*, 39:1055-1070.
- PRAKASH, S. and PANDEY, R.** (1985) Generation of Electric Fields due to the Gravity Wave Winds and their Transmission to other Ionospheric Regions. *J. Atmos. Terr. Phys.*, 47:363-374.
- RASTOGI, R.G.** (1989) The Equatorial Electrojet: Magnetic and Ionospheric Effects. "Geomagnetism" Ed. J.A. Jacobs, Academic Press, 3:461-525.
- RAVINDRAN, S. and REDDY, C.A.** (1993) Variation of Type I Plasma Wave Phase Velocity with Electron Drift Velocity in the Equatorial Electrojet. *J. Geophys. Res.*, in press.
- REDDY, C.A.** (1977) The Equatorial Electrojet and the Associated Plasma Instabilities. *J. Sci. Industr. Res. (India)*, 36:580-589.
- REDDY, C.A.** (1981) The Equatorial Electrojet: a Review of the Ionospheric and Geomagnetic Aspects. *J. Atmos. Terr. Phys.*, 43:557-571.
- REDDY, C.A.** (1989) The Equatorial Electrojet, *PAGEOPH*, 131:487-508.
- REDDY, C.A. and DEVASIA, C.V.** (1978) Equivalent Circuit Analysis of Neutral Wind Effects on Equatorial Electrojet. *Nature*, 273:195.
- REDDY, C.A. and DEVASIA, C.V.** (1981) Height and Latitude Structure of Electric Fields and Currents due to Local East-west Winds in the Equatorial Electrojet. *J. Geophys. Res.*, 86:5751-5767.
- REDDY, C.A., SOMAYAJULU, V.V. and VISWANATHAN, K.S.** (1980) The Lunar Phase and the Equatorial Electrojet. In *Low Latitude Aeronomical Processes, COSPAR Symposium Series 8*, Ed. Mitra, A., Pergamon Press, 29-32.
- REDDY, C.A., VIKRAMKUMAR, B.T. and VISWANATHAN, K.S.** (1987) Electric Fields and Currents in the Equatorial Electrojet deduced from VHF Radar Observations-I. A Method of estimating Electric Fields. *J. Atmos. Terr. Phys.* 49:183-191.

RICHMOND, A.D. (1973) Equatorial Electrojet-
I. Development of a Model including Winds and
Instabilities. *J. Atmos. Terr. Phys.*, 49:1083-
1103.

Submetido em 24.03.93
Revisado em 31.05.93
Aceito em 01.06.93
Editor responsável V.W.J.H. Kirchhoff

STENING, R.J. (1985) Modelling the Equatorial
Electrojet. *J. Geophys. Res.*, 90:1705-1719.

Key words

Winds
Waves
Equatorial Electrojet

Palavras chave

Ventos
Ondas
Eletrojato Equatorial

INTRODUCTION

The Equatorial Electrojet (EEJ) is an intense band of electric current, which flows along the magnetic equator in the E region (110-120 km) of the ionosphere. The equatorial enhancement of the ionospheric current is explained as being due to the large

vertical polarization field maintained within only a few degrees on either side of the magnetic equator, due to large gradients of the ionospheric conductivity in comparison with the horizontal conductivity of the earth. The vertical polarization field is maintained throughout by the Hall drift (crossing of the ions constituting an eastward current, which varies